A Coatable, Lightweight, Fast-response Nanocomposite Sensor for *in-situ* Acquisition of Dynamic Elastic Disturbance:

from Structural Vibration to Ultrasonic Waves

Zhihui ZENG[a,b,c] [§] [‡], Menglong LIU[a] [§] [‡], Hao XU[a] [§], Weijian LIU[a], Yaozhong LIAO[a], Hao JIN[b], Limin ZHOU[a], Zhong ZHANG[b] [**], and Zhongqing SU[a] [*]

[a]Department of Mechanical Engineering
The Hong Kong Polytechnic University, Kowloon, Hong Kong SAR

[b]CAS Key Laboratory of Nanosystem and Hierarchical Fabrication
National Center for Nanoscience and Technology, Beijing 100190, P. R. China

[c]University of Chinese Academy of Sciences (UCAS), Beijing 100049, P. R. China

Submitted to *Smart Materials and Structures*

(initially submitted on 31 December 2015; revised and re-submitted on 16 March 2016)

[§] These authors contributed equally to this work.
[‡] PhD student.
[*] Corresponding author. Email: zhongqing.su@polyu.edu.hk (Prof. Zhongqing Su, *Ph.D.*)
[**] Corresponding author. Email: zhong.zhang@nanoctr.cn (Prof. Zhong Zhang, *Ph.D.*)

Abstract

Inspired by an innovative sensing philosophy, a lightweight nanocomposite sensor made of a hybrid of carbon black (CB)/polyvinylidene fluoride (PVDF) was developed. The nano-scalar architecture and percolation characteristics of the hybrid were optimized, in order to fulfil *in-situ* acquisition of dynamic elastic disturbance from low-frequency vibration to high-frequency ultrasonic waves. Dynamic particulate motion induced by elastic disturbance modulates the infrastructure of CB conductive network in the sensor, with introduction of the tunneling effect, leading to dynamic alteration in piezoresistivity measured by the sensor. Electrical analysis, morphological characterization, and static/dynamic electro-mechanical response interrogation were implemented, to advance insight into the sensing mechanism of the sensor, and meanwhile to facilitate ascertainment of an optimal percolation threshold. At the optimal threshold (~ 6.5 wt%), the sensor exhibits high-fidelity, fast-response, and high-sensitivity to ultrafast elastic disturbance (in an ultrasonic regime up to 400 kHz) yet with an ultralow magnitude (of the order of micrometer). Performance of the sensor was evaluated, against conventional piezoelectric transducer and strain gauge, showing excellent coincidence, yet a much greater gauge factor and frequency-independent piezoresistive behaviours. Coatable to a structure and deployable in a large quantity to form a dense sensor network, this nanocomposite sensor has blazed a trail for implementing *in-situ* sensing for vibration- or ultrasonic wave-based structural health monitoring, by striking a compromise between "sensing cost" and "sensing effectiveness".

*Keywords***:** nanocomposite sensor; carbon black; polyvinylidene fluoride; structural health monitoring; vibration; guided ultrasonic waves

1. Introduction

Conductive polymer composites (CPCs), a prevailing modality of bourgeoning nanocomposites, have been increasingly explored for developing new functional and structural materials, transducers, anti-static devices, and electro-magnetic shielding [1-4]. The nanofillers of CPCs can be diverse, as typified by carbon nanotubes (CNTs) [1, 2, 5, 6], carbon black (CB) [7], carbon fibers [8], and graphene [9], to name a few. The nano-scale of the nanofillers allows them to be dispersed in polymer matrices uniformly, and the coalescence between nanofillers and polymers introduces some appealing and unique material features, such as low density, desired flexibility, easy tailorability in shape, chemical stability, and favourable electrical-mechanical performance. Of particular research interests in recent is the use of CPCs to attempt innovative sensors [1, 2, 10-26]. CPCs-based sensors are demonstrably capable of perceiving structural or ambient changes with desired sensitivity and accuracy, with successful paradigms including detection of gas leakage and content [19, 20, 22-26], measurement of static or quasi-static strains [1, 2, 13-18], acquisition of dynamic responses [21], and detection of damage [10-12].

In this backdrop, a great deal of effort has been directed to the development of CPCs-based piezoresistive strain sensors for measuring static (or quasi-static) deformation [17, 18], on which basis a diversity of applications, and damage detection in particular, can be implemented. The cardinal premise of the use of such sensors for damage detection resides in the fact that damage in a structure, to which the sensor is adhered, can amend the electrical conductivity formed by nanofillers in sensors. Representatively, a CPCs-based piezoresistive sensor composed of CNTs and polyvinylidene fluoride (PVDF) were prepared with various CNT concentrations [13, 14]. The stability and sensitivity of the senor, along with its susceptibility to ambient temperature, for strain signal acquisition, were evaluated

rigorously. In another example, multi-walled CNT thin films were fabricated by a layer-by-layer (LbL) technique [27]. The responses of the thin films to various stimuli were investigated, whereby a two-dimensional mapping of the conductivity of CNT thin films was constructed. The results are conducive to the development of a novel sensing skin. As an extension of the above work, CNT thin films were spray-deposited directly on a glass fiber composite laminate [28], and the spatially distributed electrical conductivity of the films was monitored. Upon a benchmarking processing against the voltage acquired when the laminate is in its intact status, location and severity of a low-velocity-impact-induced damage in the laminate were ascertained via an electrical impedance tomography algorithm. Compared with single-phase rigid ceramic sensing blocks (*e.g.*, lead zirconate titanate (PZT)) or conventional metallic foil-based strain gauges, CPCs-based piezoresistive strain sensors have been demonstrated more sensitive to material deformation, with additional merits such as enhanced measurement repeatability [13, 14, 27, 28].

Though effective in detecting the existence of damage, most CPCs-based piezoresistive sensors, by measuring damage-caused changes in electrical resistance (ER), are confronting by inherent bottlenecks including that

(i)   the change in ER, measured by a pair of electrodes, is a global indicator to reflect the holistic material properties between the two electrodes, and therefore it offers limited information at a *qualitative* level – likely indicating the existence of damage beneath the sensor only – that is because the damage out of the coverage of a sensor would not alter ER measured by that sensor;

(ii)   even with extended coverage, a sensor is still unwieldy to spatially locating damage beneath it, let alone its use for quantitative assessment of damage (including location and severity parameters). That is because the measured ER change is a uniform value

across two electrodes, regardless of the discrepancy in location and severity of different damage events; and

(iii)   last but not the least, most CPCs-based sensors are capable of perceiving a relatively large material deformation (of the order of *millimeter*) when the material undergoes a static or quasi-static (few hertz) load, because only when the material deformation is in such a degree could it introduce conspicuous change to the conductive networks formed by nanofillers in the sensors. This, however, is obviously not the case for ultrasonic waves (GUWs) – GUWs usually feature a loading/unloading process with an ultralow magnitude (of the order of *micrometer*), yet in an ultrasonic frequency regime.

Restricted by these factors, the majority of existing CPCs-based sensors, by exploring changes in the conductive networks formed by nanofillers, may not accommodate the needs from *quantitative* damage detection in which not only the existence of damage but its location and severity are expected to be evaluated, although CPC-based sensors hold a promise to implement *in-situ* signal acquisition.

Motivated by this and enabled by recent advances in nanotechnology, sensor technique, and electronic packaging, a nano-engineered, lightweight CPCs-based nanocomposite sensor made of a hybrid of CB and PVDF was developed, for implementing damage detection and structural health monitoring (SHM) which take advantage of dynamic elastic disturbance. Here, the dynamic elastic disturbance refers to either global structural vibration signatures (e.g., eigen-frequencies, modal curvatures, mechanical impedance or damping [29]) or local GUW features (e.g., arrival time, phase delay, amplitude change) [30-38]. In the sensor, CB nanofillers serve as the reinforcement, while PVDF as matrix, to optimally form a conductive

5

network. Electrical analysis, morphological characterization, and static/dynamic electro-mechanical response investigation were performed, to advance insight into the tunneling effect in the formed conductive network when the sensor is in response to dynamic elastic disturbance. An optimal percolation threshold of the CB network was ascertained, in order to achieve favourable sensitivity to dynamic signals from low-frequency vibration to high-frequency GUWs in the range of hundreds of kilo-hertz, yet with ultralow magnitude. To examine the correctness, sensitivity and accuracy of the fabricated nanocomposite sensor, captured vibration and GUW signals were compared with the counterpart signals acquired by conventional piezoelectric transducers and strain gauges. Coatable to a structure and deployable in a large quantity to configure a dense sensor network, this lightweight nanocomposite sensor is conducive to *in-situ* sensing towards SHM.

2. Sensor Fabrication and Characterization

2.1 Material Preparation

CB (N220, with an average particle diameter of 80 nm, supplied by CABOT Corporation) was chosen as the nanofiller, while PVDF (Kynar k721, with a density of 1.74 g/cm^3 and a melting point of ~158 ℃, supplied by ARKEMA) as the matrix, to fabricate a nanocomposite hybrid. The rudimental consideration of using CB as the nanofiller and PVDF as matrix lies in a twofold fact: (i) CB has a nano-scalar size and high specific surface area with PVDF, and it, compared with other nanofiller candidates such as CNTs, features much reduced amount of entanglement of nanoparticles [39-41], beneficial to the formation of an even, stable and uniform conductive network; (ii) PVDF, a thermoplastic material with higher elastic modulus, can present faster response to dynamic change than traditional rubber-based piezoresistive materials (rubber-based often exhibiting complex time- and frequency-dependent viscoelastic properties, restricting them from being responsive to fast-change

signals). Such a property of PVDF makes the hybrid highly responsive to dynamic elastic disturbance without marked hysteresis (to be demonstrated in sequent experiment). In addition, PVDF possesses other merits including low-density, chemical inertness, thermal stability, easy-processing, and flexibility [13, 14, 42]. Altogether, CB and PVDF endow the fabricated nanocomposite hybrid with enhanced sensitivity and high-fidelity response to dynamic changes applied to the formed conductive network.

A standard melt-mixing process was applied to disperse CB nanofillers into PVDF in an internal mixer at 190 ºC and 50 rpm for 0.5-hour. A variety of mass ratios of CB nanofillers to PVDF in the hybrid, ranging from 5 to 30 wt%, was considered during preparation. The fabricated nanocomposite hybrid was immobilized between two steel plates and molded to films ~200 µm in the thickness, using a standard hot-pressing process in which each film was hot-pressed at 20 MPa and 190 ºC for 10-minute, and then cooled to a room temperature at an atmospheric pressure for another 60-minute. Upon curing, the nanocomposite films were tailored to rectangular flakes, each measuring 15 mm × 10 mm (thickness remained at ~200 µm). To introduce electrodes to each flake to configure a sensor, each flake was silver pasted using a dual-component (polymer/silver powder) adhesive (D05001, Beijing Emerging Technology Co. Ltd., China) with shielded cables. The ER of each sensor with silver pasted electrodes was measured, and found similar to the intrinsic ER of a raw flake prior to electrode installation; moreover, no discernible discrepancy in measured ER using the sensors from the same batch could be observed. Both imply a good fabrication process of the sensor and proper installation of electrodes. A sensor with two electrodes in its final fashion is photographed in Figure 1. Small and lightweight, such a sensor can be produced in a single fabrication process, and deployed in a large quantity for configuring a sensor network.

Figure 1 A fabricated CB/PVDF nanocomposite sensor with silver pasted two electrodes

(front and back view)

2.2 Sensor Characterization

2.2.1 Electrical Analysis

To ascertain the conductivity of the fabricated nanocomposite hybrid at each CB weight ratio, ER of each sensor was measured using a standard four-probe method with a semi-conductor characterization system (4200-SCS, Keithley Instrument, Inc., Cleveland, Ohio, the USA) at a room temperature. With ascertained ER (R), the electrical conductivity (denoted by σ) was defined by $\sigma = \dfrac{l}{R \times A}$, where A and l are the effective area and length between two electrodes of a sensor, respectively. The accordingly obtained average σ (Siemens per meter, S/m) at representative CB weight ratios (5, 6.5, 8, 10, 20 and 30 wt%) are listed in Table 1 and plotted in Figure 2, both revealing that a dramatic change in conductivity of the sensor takes place when the CB weight ratio is between 5 and 8 wt%, in which even a slight increase in CB weight ratio can lead to significant alteration in the conductivity of the sensor.

Table 1 Average conductivity (σ) of the fabricated CB/PVDF nanocomposite sensors

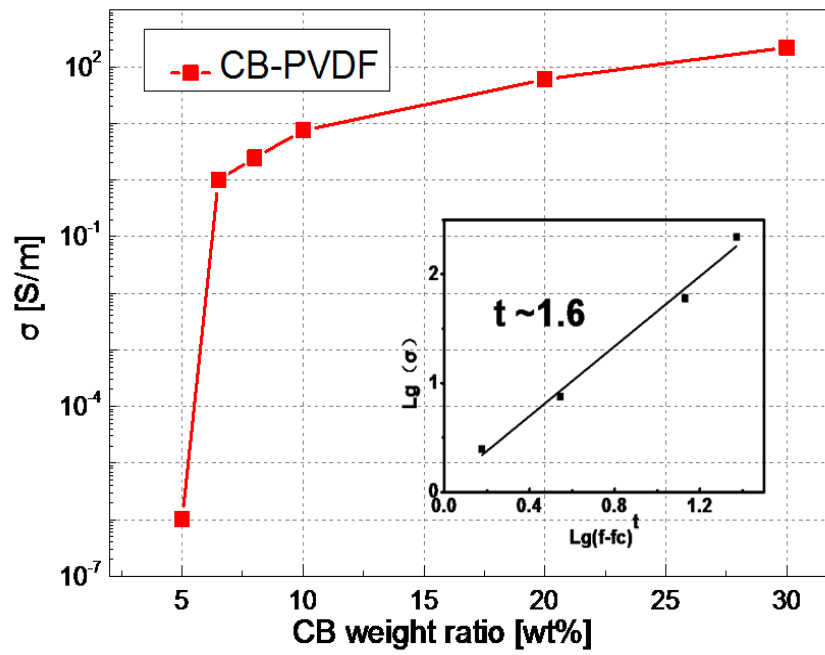| Contents of CB [wt%]	σ [S/m]
5	1.0×10^{-6}
6.5	1.0
8	2.5
10	7.5
20	60
30	220

Figure 2 Average conductivity (σ) of the fabricated CB/PVDF nanocomposite sensors at different CB weight ratios (insert: log–log plot between σ and *f* pairs with linear fitting for determination of percolation threshold)

In both Table 1 and Figure 2, a marked increase in electrical conductivity of the hybrid by a six-order of magnitude can be observed at 5~8 wt%, this indicating the formation of a fully conductive CB network in the sensor at this particular CB weight ratio. On the basis of this, 5~8 wt% of CB content in the hybrid is deemed a vicinity of the percolation threshold of the CB conductive network. The percolation threshold [43, 44] represents a transition of the hybrid from insulation to conduction, beyond which a slight increase in CB content can give rise to a tremendous leap in the number of conductive paths formed by dispersed CB nanofillers and consequently an abrupt increase in conductivity of the sensor.

To ascertain the exact percolation threshold (denoted by f_c) in the above-determined vicinity range of 5~8 wt%, *Percolation Theory* was recalled [43, 44], in which σ of the sensor is defined as

$$\sigma \propto \left(f - f_c\right)^t, \qquad when \quad f > f_c \tag{1}$$

where f signifies the fraction of conductive nanofillers (viz., CB in this study) obtained from a series of measurement, f_c the percolation threshold to be determined, and t the critical exponent depending on the nanofillers-formed conductive network. Using Eq. (1), f_c was derived by applying a linear fitting on a series of measured σ and f pairs (as seen in the log–log plot in the insert of Figure 2). Upon linear fitting, f_c and t of the fabricated nanocomposite hybrid were found to be ~6.5 wt% and 1.6, respectively.

2.2.2 Morphological Characterization

To gain insight into the nano-scalar architecture of the formed CB conductive network when the sensor is subject to elastic disturbance, morphological characterization was implemented on the hybrid using a scanning electron microscopy (SEM) (JSM-7500F, JEOL Ltd.). First,

the hybrid was fractured into small-sized samples (with a thickness of ~200 μm for each) in liquid nitrogen. Sputter coating was applied on cryo-fractured surface of each sample with a thin layer of gold. The obtained SEM images, at several representative CB weight ratios, are displayed in Figure 3. It can be observed that CB nanofillers are dispersed in PVDF randomly and evenly throughout all the weight ratios, this implying a good fabrication process of the sensor. In particular, at the determined percolation threshold (~6.5 wt%), Figure 3(b), it is apparent that a substantial number of conductive paths have been created in the CB network owing to dramatically increased connections among CB nanofillers and their aggregations. This yields an instantaneous transition from insulative to conductive status of the sensor, compared with other cases in which CB contents are below the percolation threshold (e.g., Figures 3(a)). On the other hand, with higher CB weight contents beyond the percolation threshold (e.g., 20 wt% in Figure 3(c), and 30 wt% in Figure 3(d)), CB network is densified and CB nanofillers tend to be saturated in the matrix; no further increase in conductivity can be measured in comparison with the case at ~6.5 wt%. These observations from SEM images coincide with the percolation threshold of ~6.5 wt% previously determined using the Percolation Theory.
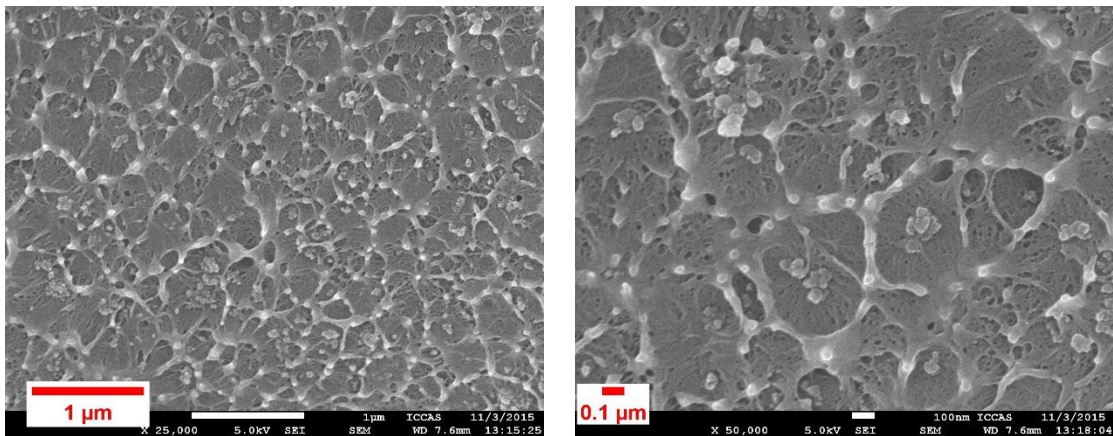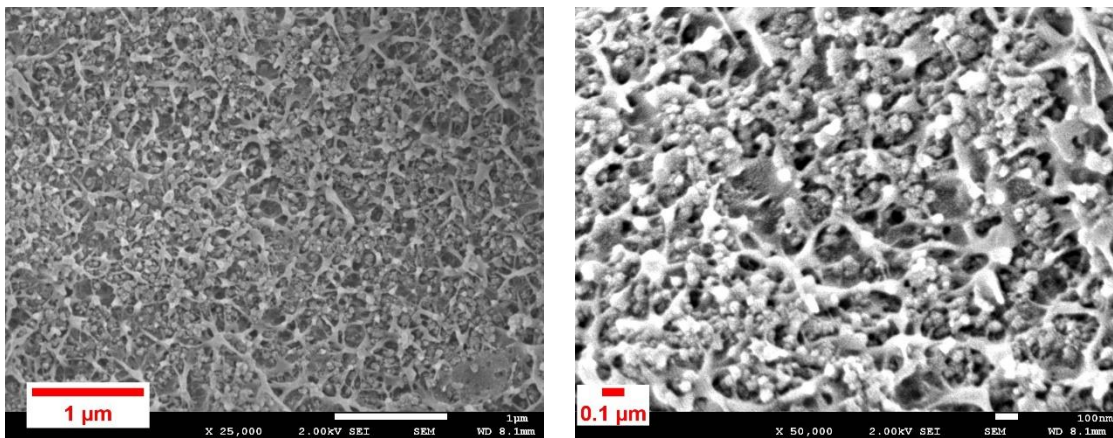

(a)
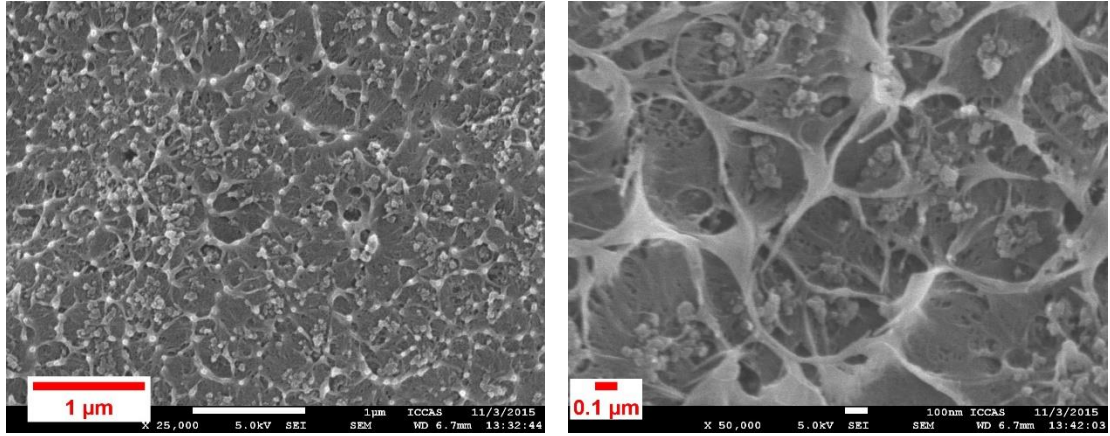
(b)
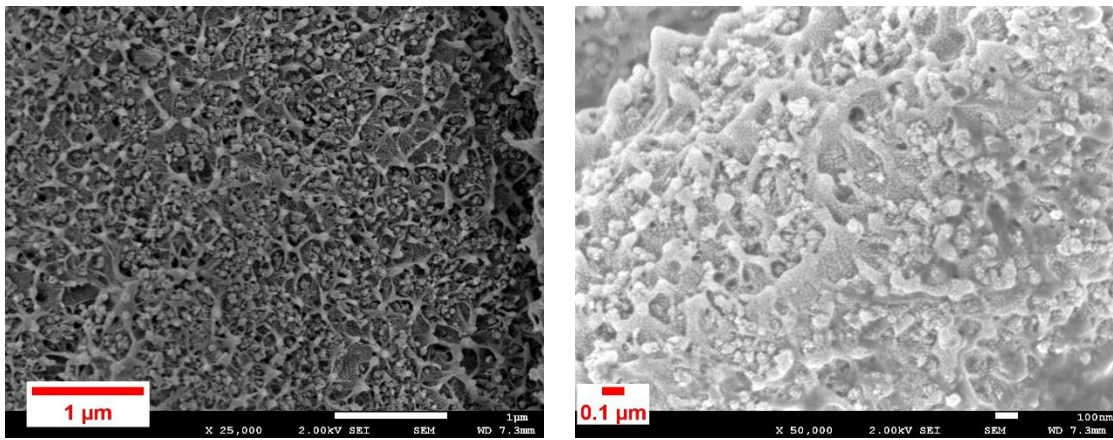
(c)

(d)

Figure 3 Nano-scalar structures of the fabricated CB/PVDF nanocomposite sensors at different CB weight ratios: (a) 5, (b) 6.5, (c) 20, and (d) 30 wt% (right: zoomed-in SEM image of the one on left)

X-ray diffraction (XRD) analysis was further carried out on the hybrid at a room temperature on a XRD platform (X'Pert Pro, PANalytical, the Netherlands), with a specular reflection mode (Cu Ka radiation [45]) and a scanning angle varying from 15° to 29° (with a scanning rate of 4° s^{-1}). A typical XRD pattern, at the determined percolation threshold (~6.5 wt%) is displayed in Figure 4(a).
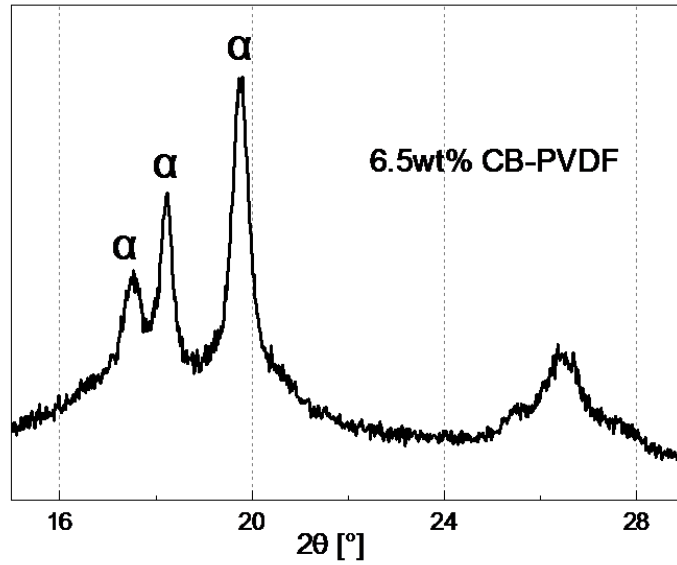
(a)
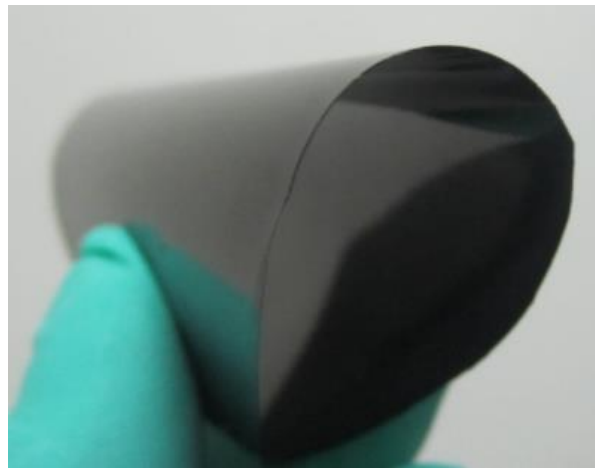
(b)

Figure 4 XRD pattern of the fabricated CB/PVDF nanocomposite sensors (2θ: scanning

angle)

13

XRD results argue that the fabricated hybrid possesses a characteristic pattern of α-crystals and therefore features a non-polar crystal structure. This speculation excludes the possibility that the piezoresistivity manifested by the sensors could originate from the PVDF matrix itself, rather than the CB conductive network induced by external dynamic elastic disturbance. This is because: only a polar crystal (such as β-crystals) can lead to piezoelectricity (as interpreted elsewhere [13, 14, 42, 43]); given the fabricated sensor features a non-polar crystal structure, the PVDF matrix in the hybrid would not cause prominent piezoelectricity; once change in conductivity of the sensor detected, it can be fully attributed to the consequence of the change in the CB conductive network caused by dynamic elastic disturbance (rather than PVDF itself). In addition, optical images, as seen in Figure 4(b), reveal good flexibility of the sensor, highlighting the capacity of the sensor in adapting to non-flat structural surfaces – an intriguing merit of the sensor towards practical engineering applications.

2.2.3 Static/Dynamic Electro-mechanical Response Interrogation

Take a step further to advance the understanding of the sensing mechanism of the sensor when subjected to static and dynamic elastic disturbance, static/dynamic electro-mechanical responses of sensors at various CB weight ratios were evaluated with a dynamic mechanical testing platform (TA Q800, TA Instruments) and a semi-conductor characterization system (4200-SCS, Keithley Instrument, Inc., Cleveland, Ohio, the USA).

Static

Figure 5 shows the change ratio of measured ER of the sensors against static load-induced strain. For comparison, the change ratio of a typical metal-foil strain gauge is also included in the figure.
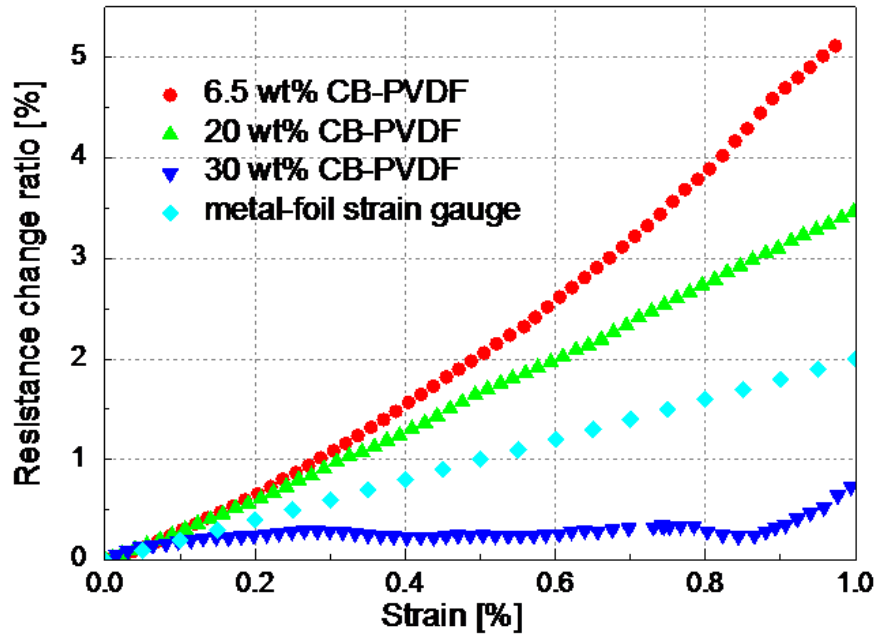
Figure 5 Change ratio of measured ER of the fabricated CB/PVDF nanocomposite sensors at different CB weight ratios under static load

As observed, at a given strain, the lower the CB weight ratio of the hybrid, the higher the change ratio of ER it is, and therefore the higher a gauge factor of the sensor. As discussed earlier, the nano-scalar architecture of CB nanofillers allows a high specific surface area of evenly dispersed nanofillers in PVDF once a conductive network formed, and this can advance the sensing sensitivity of the sensor to strain, due to a consequence of the breakage of the network and the introduction of tunneling effect [15, 16, 27]. As demonstrated elsewhere [15, 16, 27, 46], the tunneling effect is dominant when the nanofiller or adjacent building block is in a close proximity (of the order of several nano-meters) but not in direct contact with the each other. In particular, when the strain is not at a significant degree (such as the low strain induced by ultrasounds), the tunneling effect is considered to be the key mechanism leading to the change in the conductivity of the sensor.

A further increase in CB content only densifies conductive paths in a saturated conductive network, and a saturated network is not prone to be affected by further increase in strain (not giving rise to increase in gauge factor). Therefore, a higher CB content (such as 30 wt%) of the hybrid leads to a smaller change ratio of ER (therefore a lower gauge factor), compared with a lower CB content (such as 6.5 wt%). This has, using another means, corroborated the percolation threshold determined previously. By calculating the ratio of resistance change to strain, the gauge factor of the fabricated sensor was calculated to be 5.0 ± 0.6 (at ~6.5 wt%) – much higher than that of a metal-foil strain gauge which is usually ~2 [15] (as seen in Figure 5). The high gauge factor guarantees superior sensitivity of the sensor to small strains – the case of GUWs (GUWs usually features a weak magnitude of the order of several micro-strains).

Dynamic

By extending the static loading in the above to dynamic loading using the same testing platform, the sensor was applied with a cyclic load windowed in a ramp strain mode with a ramp rate of 1.0%/min until reaching its maximum at 1.0%. As a representative result, the change ratio of ER measured by the sensor at the percolation threshold (~6.5 wt%), when subjected to the applied cyclic load, is displayed in Figure 6, to observe a high consistence between the response and the applied cyclic load without discernable hysteresis, this asserting good dynamic stability and desirable measurement repeatability of the sensor.

Very importantly, the observed reversibility of the sensor response under a cyclic load corroborates the conclusion drawn earlier that under small strains (e.g., GUWs), the dominant sensing mechanism of the sensor is the tunneling effect among nanofillers, instead of the loss of contact or breakage of conductive network. This is because the loss of contact
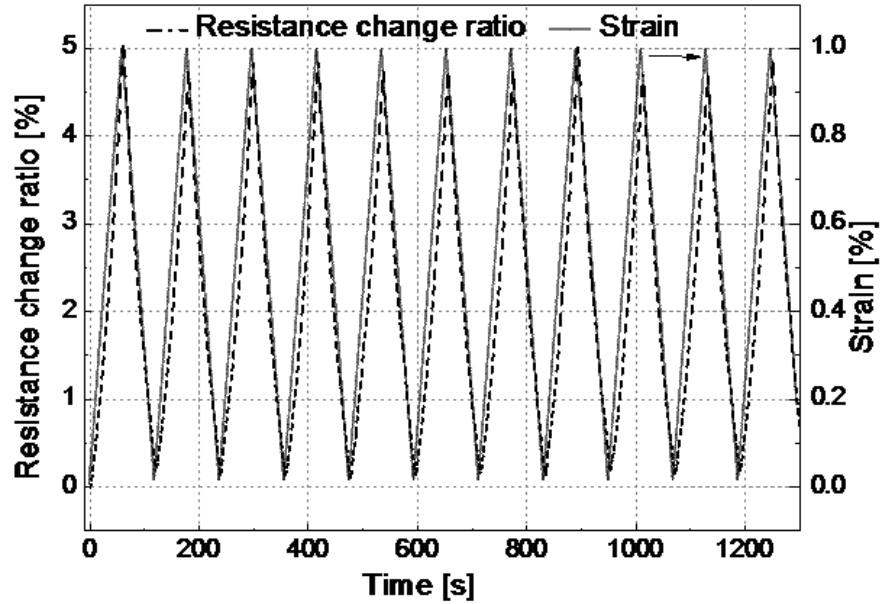
Figure 6 Electro-mechanical response of the fabricated CB/PVDF nanocomposite sensors in comparison with applied cyclic load (at percolation threshold)

Both the static and dynamic electro-mechanical response interrogation have demonstrated that the fabricated sensor, at the determined percolation threshold, possesses a capacity of perceiving material deformation under static or dynamic loads, with reversibility yet without hysteresis. Such an attribute of the sensor can be attributable to the tunneling effect, accompanied with loss of contact among nanofillers thought not dominant – a property to be exploited for acquisition of dynamic structural vibration and GUWs in what follows.

3. *In-situ* Acquisition of Dynamic Elastic Disturbance

The feasibility, correctness, and sensitivity of using the fabricated CB/PVDF nanocomposite sensors to perceive dynamic elastic disturbance was examined, ranging from low-frequency structural vibration to high-frequency GUWs. On the basis of previous material characterization, the sensor with a percolation threshold of ~6.5 wt% was selected for the sake of its highest gauge factor. Lightweight and small, the sensor can be conveniently and quickly surface-glued on or embedded in a structure to implement *in-situ* signal acquisition, without introducing obvious weight and volume penalty to the host structure.

### 3.1 Dedicated Signal Amplification and Acquisition System

Owing to weakness of the magnitude of elastic disturbance and particularly that of GUWs in a frequency range of kilo- or mega-Hertz (GUW-induced elastic disturbance is usually of the order of several micro-strains), signals captured by the sensors are envisaged to be prone to contamination from ambient noise and uncertainties, and this, under most circumstances, leads to a low signal-to-noise ratio (SNR). To circumvent this, a self-contained signal amplification and acquisition system was developed, to be used in conjunction with the sensors. The system embraces a signal amplification module and a signal generation/acquisition module developed on a PXI (PCI eXtensions for Instrumentation) bus platform (NI® PXIe-1071).

The amplification module integrates a Wheatstone bridge with resistors compatible to the ER of the selected sensor (ER was ascertained via electrical analysis detailed in Section 2.2.1), an electronic amplifier circuit, a series of filters and a signal conversion unit (for converting measured piezoresistivity to electrical voltage signals). The signal generation/acquisition module consists of an electro-mechanical shaker (B&K® 4809) (for

introducing vibration to a structure), a waveform generator (NI® PXIE-1071) (for exciting GUWs via PZT wafers (Physik Instrumente Co., Ltd., PIC151; diameter: 9 mm; thickness: 0.5 mm)), a linear power amplifier (Ciprian® US-TXP-3), and an oscilloscope (Agilent® DSO9064A). Using these two modules, structural vibration and GUW signals were generated and then captured.

3.2 Low-frequency Structural Vibration

A cantilevered glass fiber-epoxy composite beam (290 mm long, 38 mm wide and 2 mm thick) was prepared, to which a nanocomposite sensor and a strain gauge sensor (for comparison) were surface-attached using an instant glue (Aron Alpha® HHI-11485). The central position of the sensor was measured 70 mm from the clamped end of the beam, as seen in Figure 7. The shaker excited the beam through a point 270 mm from the clamped end, with a sinusoidal signal sweeping between 100 to 2000 Hz.
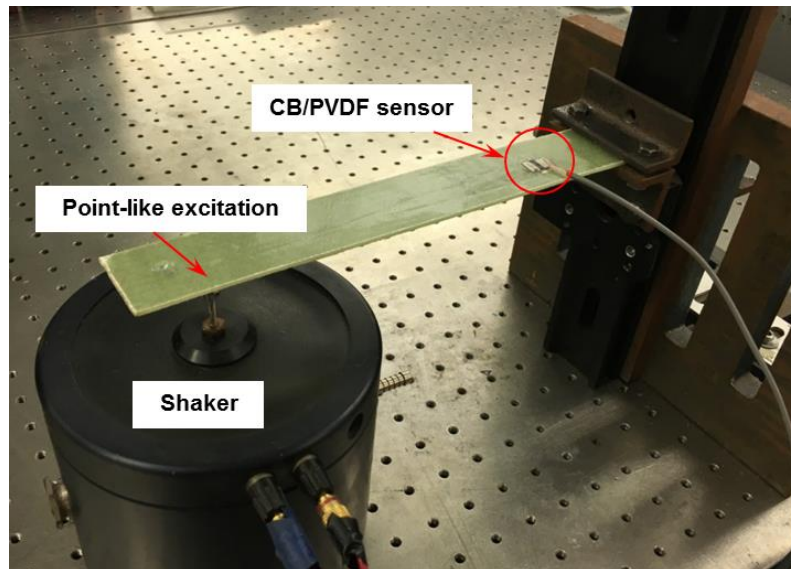
(a)
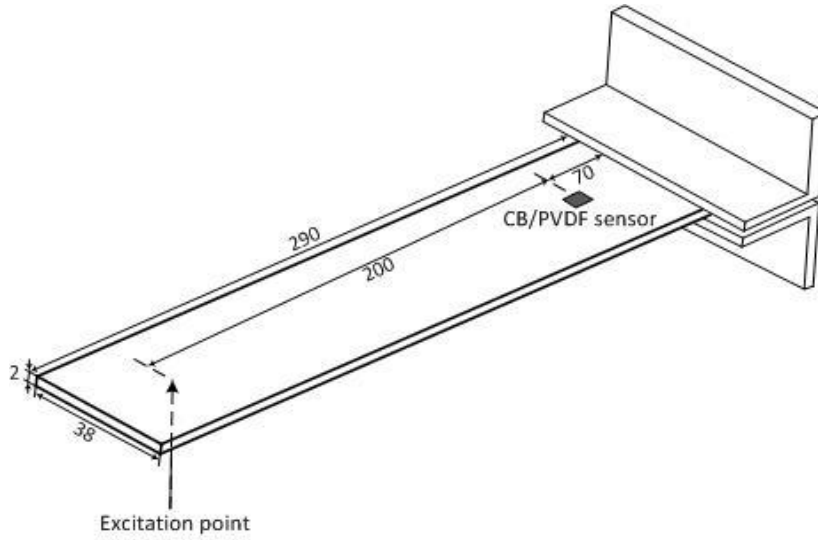
(b)

Figure 7 (a) Photographed and (b) schematic of the experimental set-up for acquisition of

low-frequency vibration of a glass fiber-epoxy composite beam (unit: mm)

To facilitate better understanding of the signals captured by the sensor, bandpass filters were designed and applied on raw signals, to screen measurement noise. All captured signals were averaged for 16 times to remove random noise and uncertainties. The signals, acquired at the three representative frequencies (100, 500 and 2000 Hz) are presented in Figures 8(a) to (c), respectively, to observe good repeatability of the sensor response. Besides, discrepancy in signal phase between the responses acquired by the CB/PVDF sensor and the strain gauge is barely discerned in Figure 8(c), extrapolating that the hysteresis of the fabricated sensor, in response to dynamic elastic disturbance up to 2000 Hz, is unperceivable. In a previous study, a rubber-based piezoresistive sensor was used to measure the piezoresistive response of a similar case, but to observe certain delay of the response to excitation, and such delay generally increases with frequency of applied pressures due to the intrinsic viscoelastic properties of rubbers [21]. This has echoed the previous justification pertaining to the

20

selection of PVDF as the matrix of the sensor – the high elastic modulus of the PVDF drives the sensor to be responsive to dynamic disturbance without marked hysteresis.

Furthermore, by adjusting the magnitude of excitation, the accordingly acquired signals, at 100 Hz and 2000 Hz, are compared in Figure 8(d), to remark a good linear correlation between the excitation and response. This observation surmises an approximately linear response of the nanocomposites sensor to dynamic elastic disturbance (up to the discussed frequency of 2000 Hz). In addition, the minute error bar in Figure 8(d) accentuates the stability of the sensor in performing different measurements.
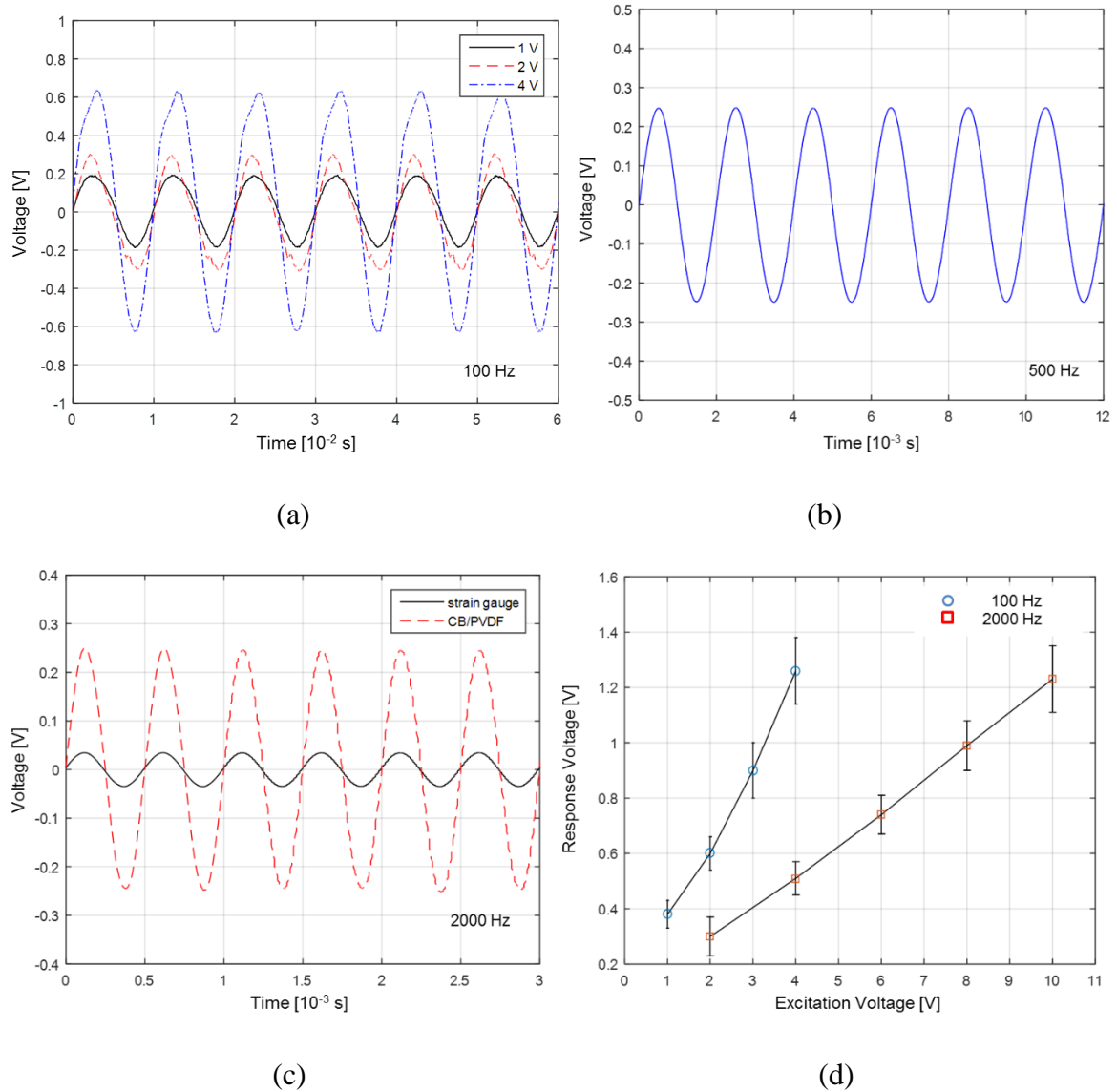

(a)

(b)

(c)

(d)

Figure 8 Vibration signals captured by the fabricated CB/PVDF nanocomposite sensor (a) with different excitation magnitudes (at 100 Hz), (b) at 500 Hz and (c) and strain gauge sensor (at 2000 Hz) and (d) signal amplitudes with different excitation magnitudes (at 100 Hz and 2000 Hz)

3.3 High-frequency GUWs

In the above, barely discerned discrepancy in phase between the responses acquired by CB/PVDF and strain gauge extrapolates that the hysteresis of the fabricated sensor, in response to dynamic elastic disturbance up to 2000 Hz, is unperceivable. Subsequently, performance of the sensor was examined in an ultrasonic regime. A glass fiber-epoxy composite laminate panel (600 mm$\times$ 600 mm $\times$ 2 mm) was prepared, as shown in Figure 9. To activate GUWs into the panel, two PZT wafers, denoted by PZT_1 and PZT_2, respectively, were surface-mounted on the laminate with their respective locations specified in Figure 9. Each PZT wafer served a dual-role of being actuator and receiver, respectively, in terms of piezoelectricity. Eight nanocomposite sensors were surface-glued on the laminate, on the same side of the laminate as two PZT wafers, to form a sensor network with a coverage area of 300×300 mm^2.
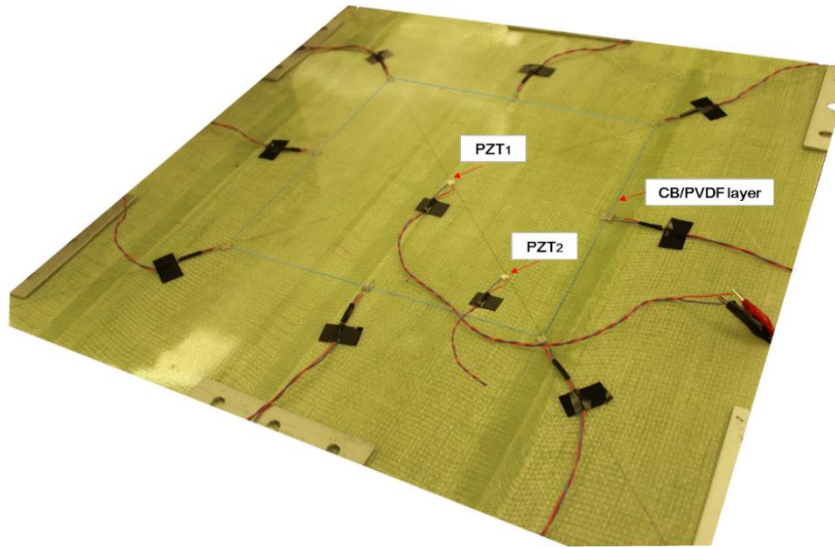
(a)
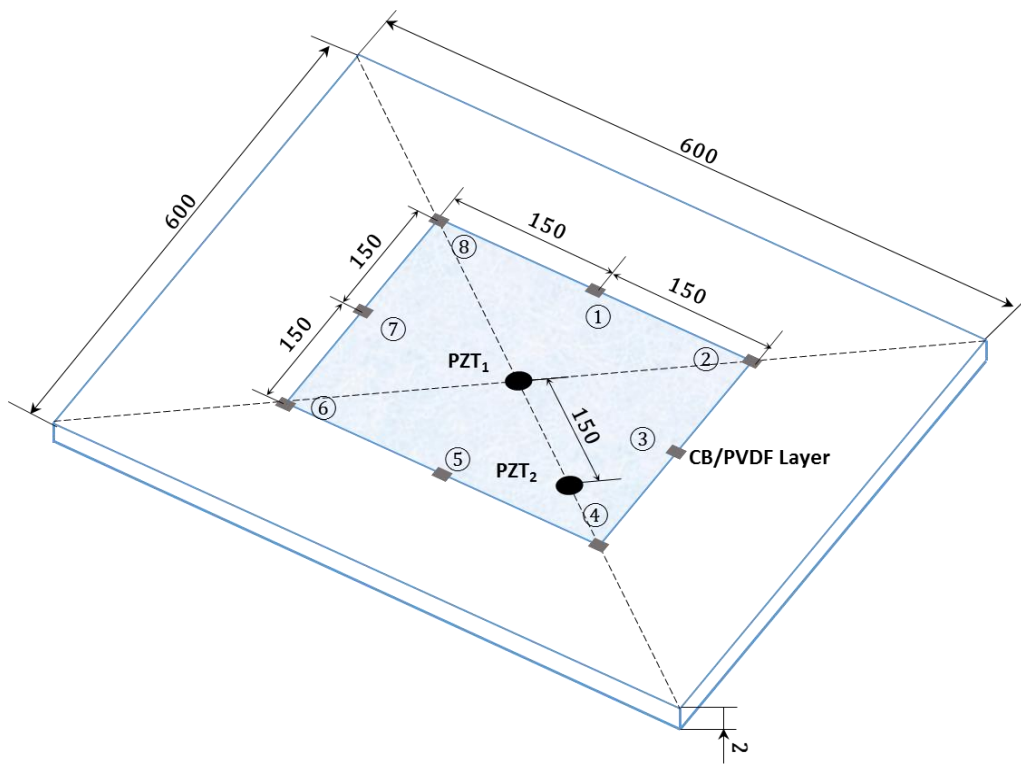
(b)

Figure 9 (a) Photographed and (b) schematic of the experimental set-up for acquisition of

high-frequency GUWs propagating in a glass fiber-epoxy composite laminate panel (unit:

mm)

Five-cycle *Hanning*-windowed sinusoidal tonebursts at a central frequency varying from 50 to 400 kHz were generated by the waveform generator, amplified to 400 Vp-p via the linear power amplifier, and then applied on PZT_1 to excite GUWs. The generated GUWs propagating in the laminate were acquired by the eight sensors through the oscilloscope at a sampling rate of 10 MHz. The GUW signals were also captured in the meantime by PZT_2 for calibration. By switching the role of two PZT wafers, the above acquisition was repeated by driving PZT_2 to introduce GUWs to the laminate, while using PZT_1 for calibration.

Representatively, Figure 10 shows the raw GUW signal captured by nanocomposite sensor ① (see Figure 9), against the counterpart signal collected by PZT_2, when PZT_1 served as the actuator to generate GUWs at 175 kHz. In the figure, the first-arrival wave components (viz., the zeroth-order symmetric Lamb wave mode guided by the laminate, denoted by S_0) perceived by both the nanocomposite sensor and PZT wafer are observed to be coincident in terms of the arrival time. The difference in respective magnitudes can be attributed to the distinguishably different sensing mechanisms of the two types of sensors: PZT wafer is a piezoelectric sensor, while the nanocomposite sensor is a piezoresistive sensor by exploring variation in a formed CB conductive network with induced tunneling effect. In all signals, crosstalk and noise components are evident. The crosstalk, observed right at the initial moment (zero moment) when a signal is excited, is a very common phenomenon in acquisition of ultrasound signals, which originates from the use of a high voltage power amplifier involved in the signal acquisition system. The crosstalk is not detrimental to signal processing and interpretation. To mitigate noise, a first-order Butterworth filter was designed and applied to all raw signals. Figure 11 shows the filtered signals presented in Figure 10, facilitating explicit recognition of the S_0 mode.

In addition, all the nanocomposite sensors in the sensor network show high consistence in performance in the discussed frequency range (50~400 kHz), implying the independence of the piezoresistive behaviours evidenced by the sensor on the frequency of dynamic elastic disturbance.

4. Further Development

With respective merits and demerits, a variety of sensors is readily available for damage detection and SHM (e.g., PZT, fiber Bragg grating, and macro fibre composites). In practical implementation, a number of spatially distributed sensors are often networked to configure a sensor network. By "communicating" one another, the networked sensors holistically and collectively perceive changes in ambient and host structures, meanwhile warranting desired redundancy of data acquisition. During sensor network configuration, a paramount target is to compromise "sensing cost" with "sensing effectiveness" – to acquire the most information with the fewest sensors. Owing to its distributed nature, a sensor network comprised of a limited number of distributed sensors (such as PZT) is likely to "overlook" information, more or less, create "blind zones", and deliver inaccurate or even erroneous results.
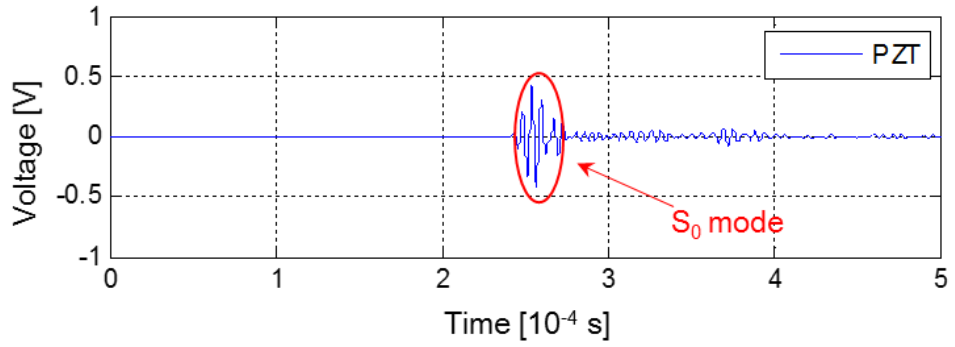

(a)

25
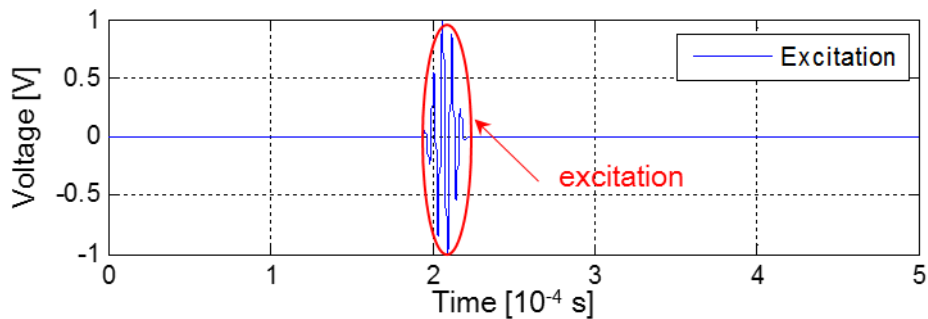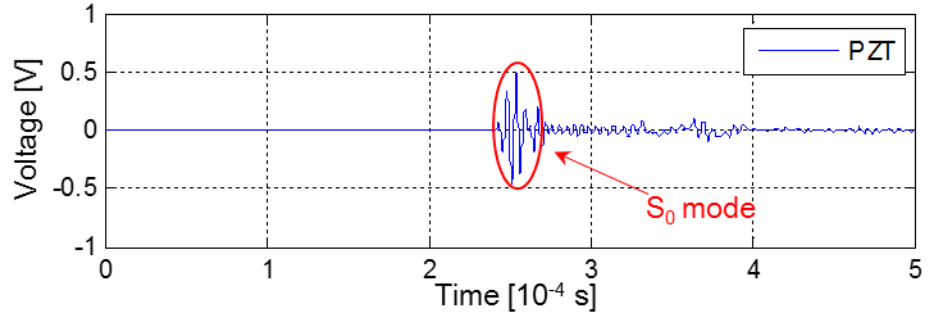
(b)
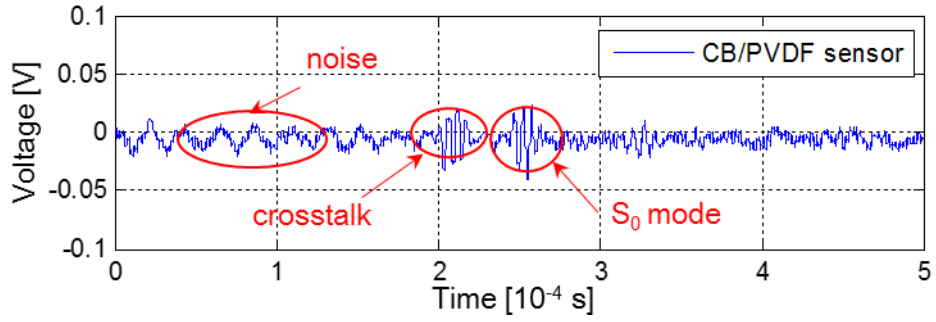
(c)

Figure 10 (a) Excitation signal (at 175 kHz); raw GUW signals captured by (b) PZT wafer

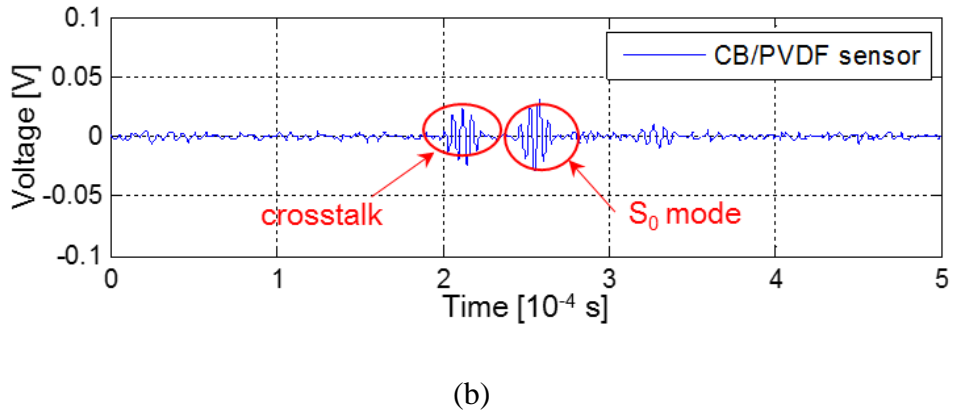(PZT$_2$), and (c) CB/PVDF nanocomposite sensor (sensor ①)

(a)

(b)

Figure 11 Noise-filtered signals shown in Figure 10 by (a) PZT wafer (PZT₂), and (b) CB/PVDF nanocomposite sensor (sensor ①)

Lightweight and small, the nanocomposite sensor developed in this study can be coated to a structure and deployed in a large quantity to form a dense sensor network, so as to address a concept of "quasi-dispersed sensing network" and allow acquisition of rich information that would be very difficult to achieve using a conventional sensor network with sparsely distributed sensors (e.g., PZT). Diverse sensor networks can be configured conveniently and quickly, by flexibly coating a certain number of such sensors. This flexibility is not restricted by the material (metals or composites) or geometric (flat or curved) traits of the host structure to be coated. Advanced processing and molding methods including screen printing, casting and other deposition methods, are currently under investigation of the authors, showing promise to implement a "quasi-dispersed sensing network", to be reported in near future. Featuring these merits, the developed nanocomposite sensor has a potential to achieve a desirable balance between "sensing cost" and "sensing effectiveness".

5. Concluding Remarks

A lightweight nanocomposite sensor made of a hybrid of CB/PVDF was developed, to fulfill *in-situ* acquisition of dynamic elastic disturbance from low-frequency vibration to high-frequency ultrasonic waves. This is the first time that a nanocomposite sensor responsive to dynamic disturbance up to 400 kHz has been documented. Via rigorous material characterization including electrical, morphological and static/dynamic electro-mechanical response interrogation, the nano-scalar architecture of the sensor was optimized to reach a desired percolation threshold of the CB conductive network (~6.5 wt%), which has been demonstrated sensitive to dynamic elastic disturbance in an ultrasonic regime up to ~400 kHz with a magnitude as low as in the order of micrometer. The sensor also presents frequency-independent piezoresistive behaviours. This study has also revealed that the tunneling effect among nanofillers dominates the sensing mechanism of the sensor in perceiving dynamic particulate motion when a CB nanofiller is in a close proximity but not in direct contact with the others. In conjunction with a dedicated signal amplification apparatus, the feasibility, correctness and sensitivity of the sensor was examined, against conventional piezoelectric transducers and metal foil strain gauge sensors, to demonstrate excellent coincidence between two types of sensors. Additionally, the sensor shows a much larger gauge factor than conventional strain gauges, therefore rendering enhanced sensitivity to weak dynamic signals. Coatable to a structure and deployable in a large quantity, this new type of nanocomposite sensor has blazed a trail for implementing *in-situ* sensing for vibration- or ultrasonic wave-based damage detection and SHM, by striking a compromise between "sensing cost" and "sensing effectiveness", while avoiding the shortcomings associated with the use of distributed sensors (*e.g.*, PZT), for instance the insufficient acquisition of information, and the adverse effects of bondline.

Acknowledgments

References

[1]   Hwang S-H, Park H W, Park Y-B 2013 Piezoresistive behavior and multi-directional strain sensing ability of carbon nanotube–graphene nanoplatelet hybrid sheets *Smart Mater Struct* 22 015013

[2]   Parmar K, Mahmoodi M, Park C, Park S S 2013 Effect of CNT alignment on the strain sensing capability of carbon nanotube composites *Smart Mater Struct* 22 075006

[3]   Gong L, Kinloch I A, Young R J, Riaz I, Jalil R, Novoselov K S 2010 Interfacial stress transfer in a graphene monolayer nanocomposite *Adv Mater* 22 2694-7

[4]   Thomassin J-M, Jérôme C, Pardoen T, Bailly C, Huynen I, Detrembleur C 2013 Polymer/carbon based composites as electromagnetic interference (EMI) shielding materials *Mat Sci Eng R* 74 211-32

[5]   Yu M 2000 Strength and breaking mechanism of multiwalled carbon nanotubes under tensile load *Science* 287 637-40

[6]   Hwang S-H, Park H W, Park Y-B, Um M-K, Byun J-H, Kwon S 2013 Electromechanical strain sensing using polycarbonate-impregnated carbon nanotube–graphene nanoplatelet hybrid composite sheets *Compos Sci Technol* 89 1-9

[7]   Yazdani H, Hatami K, Khosravi E, Harper K, Grady B P 2014 Strain-sensitive conductivity of carbon black-filled PVC composites subjected to cyclic loading *Carbon* 79 393-405

[8]   Al-Saleh M H, Sundararaj U 2009 A review of vapor grown carbon nanofiber/polymer conductive composites *Carbon* 47 2-22

[9]   Wen B, Cao M, Lu M, Cao W, Shi H, Liu J, et al. 2014 Reduced graphene oxides: light-weight and high-efficiency electromagnetic interference shielding at elevated temperatures *Adv Mater* 26 3484-9

[10]   Gao L, Thostenson E T, Zhang Z, Chou T-W 2009 Sensing of damage mechanisms in fiber-reinforced composites under cyclic loading using carbon nanotubes *Adv Funct Mater* 19 123-30

[11]   Sebastian J, Schehl N, Bouchard M, Boehle M, Li L, Lagounov A, et al. 2014 Health monitoring of structural composites with embedded carbon nanotube coated glass fiber sensors *Carbon* 66 191-200

[12]   Thostenson E T, Chou T W 2006 Carbon nanotube networks: sensing of distributed strain and damage for life prediction and self healing *Adv Mater* 18 2837-41

[13]   Ferrreira A, Rocha J G, Ansón-Casaos A, Martínez M T, Vaz F, Lanceros-Mendez S 2012 Electromechanical performance of poly(vinylidene fluoride)/carbon nanotube composites for strain sensor applications *Sensor Actuat A-phys* 178 10-6

[14]   Georgousis G, Pandis C, Kalamiotis A, Georgiopoulos P, Kyritsis A, Kontou E, et al. 2015 Strain sensing in polymer/carbon nanotube composites by electrical resistance measurement *Compos Part B Eng* 68 162-9

[15]   Hu N, Itoi T, Akagi T, Kojima T, Xue J, Yan C, et al. 2013 Ultrasensitive strain sensors made from metal-coated carbon nanofiller/epoxy composites *Carbon* 51 202-12

[16]   Hu N, Karube Y, Yan C, Masuda Z, Fukunaga H 2008 Tunneling effect in a polymer/carbon nanotube nanocomposite strain sensor *Acta Mater* 56 2929-36

[17]   Li W, Dichiara A, Bai J 2013 Carbon nanotube–graphene nanoplatelet hybrids as high-performance multifunctional reinforcements in epoxy composites *Compos Sci Technol* 74 221-7

[18]   Li W, Yuan J, Dichiara A, Lin Y, Bai J 2012 The use of vertically aligned carbon nanotubes grown on SiC for in situ sensing of elastic and plastic deformation in electrically percolative epoxy composites *Carbon* 50 4298-301

[19]   Penza M, Aversa P, Cassano G, Wlodarski W, Kalantarzadeh K 2007 Layered SAW gas sensor with single-walled carbon nanotube-based nanocomposite coating *Sensor Actuat B Chem* 127 168-78

[20]   Sivaramakrishnan S, Rajamani R, Smith C S, McGee K A, Mann K R, Yamashita N 2008 Carbon nanotube-coated surface acoustic wave sensor for carbon dioxide sensing *Sensor Actuat B Chem* 132 296-304

[21]   Qiu L, Bulut Coskun M, Tang Y, Liu J Z, Alan T, Ding J, et al. 2015 Ultrafast dynamic piezoresistive response of graphene-based cellular elastomers *Adv Mater*

[22]   Castro M, Lu J, Bruzaud S, Kumar B, Feller J-F 2009 Carbon nanotubes/poly(ε-caprolactone) composite vapour sensors *Carbon* 47 1930-42

[23]   Sadasivuni K K, Ponnamma D, Kumar B, Strankowski M, Cardinaels R, Moldenaers P, et al. 2014 Dielectric properties of modified graphene oxide filled polyurethane nanocomposites and its correlation with rheology *Compos Sci Technol* 104 18-25

[24]   Lu J, Kumar B, Castro M, Feller J-F 2009 Vapour sensing with conductive polymer nanocomposites (CPC): Polycarbonate-carbon nanotubes transducers with hierarchical structure processed by spray layer by layer *Sensor Actuat B Chem* 140 451-60

[25]   Kumar B, Feller J F, Castro M, Lu J 2010 Conductive bio-Polymer nano-Composites (CPC): chitosan-carbon nanotube transducers assembled via spray layer-by-layer for volatile organic compound sensing *Talanta* 81 908-15

[26]   Kumar B, Castro M, Feller J F 2012 Controlled conductive junction gap for chitosan–carbon nanotube quantum resistive vapour sensors *J Mater Chem* 22 10656-10664

[27]   Hou T-C, Loh K J, Lynch J P 2007 Spatial conductivity mapping of carbon nanotube composite thin films by electrical impedance tomography for sensing applications *Nanotechnology* 18 315501

[28]   Loyola B R, Briggs T M, Arronche L, Loh K J, La Saponara V, O'Bryan G, et al. 2013 Detection of spatially distributed damage in fiber-reinforced polymer composites *Struct Health Monit* 12 225-39

[29]   Fan W, Qiao P 2011 Vibration-based damage identification methods: a review and comparative study *Struct Health Monit* 10 83-111

[30]   Zhou C, Su Z, Cheng L 2011 Quantitative evaluation of orientation-specific damage using elastic waves and probability-based diagnostic imaging *Mech Syst Signal Pr* 25 2135-56

[31]   Coverley P T, Staszewski W J 2003 Impact damage location in composite structures using optimized sensor triangulation procedure *Smart Mater Struct* 12 795-803

[32]   Sohn H, Lee S J 2010 Lamb wave tuning curve calibration for surface-bonded piezoelectric transducers *Smart Mater Struct* 19 015007

[33]   Wang C H, Rose J T, Chang F-K 2004 A synthetic time-reversal imaging method for structural health monitoring *Smart Mater Struct* 13 415-23

[34]   Lin B, Giurgiutiu V 2006 Modeling and testing of PZT and PVDF piezoelectric wafer active sensors *Smart Mater Struct* 15 1085-93

[35]   Croxford A J, Moll J, Wilcox P D, Michaels J E 2010 Efficient temperature compensation strategies for guided wave structural health monitoring *Ultrasonics* 50 517-28

[36]   Michaels J E 2008 Detection, localization and characterization of damage in plates with an in situ array of spatially distributed ultrasonic sensors *Smart Mater Struct* 17 035035

[37]   Zhou W, Li H, Yuan F-G 2014 Guided wave generation, sensing and damage detection using in-plane shear piezoelectric wafers *Smart Mater Struct* 23 015014

[38]   Kundu T, Nakatani H, Takeda N 2012 Acoustic source localization in anisotropic plates *Ultrasonics* 52 740-6

[39] Babu I, de With G 2014 Enhanced electromechanical properties of piezoelectric thin flexible films *Compos Sci Technol* 104 74-80

[40] Qu Y, Dai K, Zhao J, Zheng G, Liu C, Chen J, et al. 2013 The strain-sensing behaviors of carbon black/polypropylene and carbon nanotubes/polypropylene conductive composites prepared by the vacuum-assisted hot compression *Colloid Polym Sci* 292 945-51

[41] Lin L, Liu S, Zhang Q, Li X, Ji M, Deng H, et al. 2013 Towards tunable sensitivity of electrical property to strain for conductive polymer composites based on thermoplastic elastomer *ACS Appl Mater Inter* 5 5815-24

[42] Tang X-G, Hou M, Zou J, Truss R, Yang M, Zhu Z 2012 Toughening and reinforcement of poly(vinylidene fluoride) nanocomposites with "bud-branched" nanotubes *Compos Sci Technol* 72 263-8

[43] Regev O, ElKati P N B, Loos J, Koning C E 2004 Preparation of conductive nanotube–polymer composites using latex technology *Adv Mater* 16 248-51

[44] Arjmand M, Mahmoodi M, Gelves G A, Park S, Sundararaj U 2011 Electrical and electromagnetic interference shielding properties of flow-induced oriented carbon nanotubes in polycarbonate *Carbon* 49 3430-40

[45] Geng C, Wang J, Zhang Q, Fu Q 2012 New piezoelectric damping composites of poly(vinylidene fluoride) blended with clay and multi-walled carbon nanotubes *Polym Int* 61 934-8

[46] Zhao J, Wang G, Yang R, Lu X, Cheng M, He C, et al. 2015 Tunable piezoresistivity of nanographene films for strain sensing *ACS nano* 9 1622-9